Heat & Drag Assignment (CFD)

Determining the minimum possible air velocity and drag on a heated sphere to ensure the surface temperature remains below a threshold temperature

Leon Panjwani (240134987)
MAC228
01.11.25

1.1 Abstract

This study determines the minimum air velocity (U) required to cool a sphere of diameter 50 mm, constantly emitting 300 W of heat, such that its surface temperature (T_S) does not exceed the critical threshold of 650°C (923 K). This investigation was carried out to cool the sphere, but also to minimise the subsequent drag force (F_D) on the sphere, thus reducing the load placed on the aluminium support struts and the necessary fabrication costs as a result.

The analysis combined empirical and computational approaches. Empirical methods, primarily the Whitaker correlation, established a baseline requirement of $U = 17.19\ m/s$ with an estimated drag force of $F_D = 0.0720\ N$. The CFD analysis, performed using ANSYS Fluent with a combination of the $k - \omega\ SST$ turbulence model and an ideal-gas density model, provided a more physically realistic prediction. The simulations returned slightly greater results than those calculated using empirical methods; the minimum required air velocity was determined as $U = 21.76\ m/s$ and the corresponding drag force as $F_D = 0.302\ N$. This significant difference in drag was primarily attributed to the model's ability to account for varying fluid density and accurately resolve the flow separation and surface shear stresses, which are disregarded or approximated in empirical correlations.

Recommendations for system improvement include optimising the support material from aluminium to stainless steel, and implementing surface roughness to trigger the drag crisis, which was quantified to reduce the drag force by approximately half to 0.151 N. The stainless steel provides a greater resistance and structural integrity against the heat emitted by the sphere, and the reduction in drag force reduces the load placed on the struts. Other recommendations include inlet flow conditioning, streamlining the shape of the sphere, and considering the effect of radiation.

2.1 Empirical Calculations

2.1.1 Defining Fluid Properties

The objective of this section is to establish empirical, quantitative values for the minimum required velocity (U) and resultant drag force (F_D) to ensure the surface temperature of the sphere (T_s) remains below the threshold temperature; these are found in Table 1. This is achieved by using three established correlations (Ranz-Marshall, Whitaker and Raithby) and critically evaluating their differences; these heat transfer correlations are primarily used for forced convection over a sphere.

Variable	Value	Description
Q	$300\ W$	Constant heat released by sphere
D	$0.05\ m$	Sphere diameter
T_s	$923.15\ K\ (650°C)$	Maximum permissible surface temperature
T_∞	$293.15\ K\ (20°C)$	Temperature of the air flow
μ_∞	$1.825 \times 10^{-5}\ kgm^{-1}s^{-1}$	Dynamic viscosity of air at air flow temperature
μ_s	$3.973 \times 10^{-5}\ kgm^{-1}s^{-1}$	Dynamic viscosity of air at maximum permissible surface temperature

[Table 1: relevant properties and nomenclature]

Fluid properties of air (ρ, k, C_p, μ) change significantly with temperature. The film temperature (T_f) is used in convection analysis, as it is an approximation of the temperature of a fluid inside a convection boundary layer. It is calculated using Equation (1) as the average temperature between the solid surface (T_s) and the flowing fluid (T_∞).

$$T_f = \frac{T_s + T_\infty}{2} = 608.15\ K \quad (1)$$

Variable	Value	Description
C_p	$1053\ Jkg^{-1}K^{-1}$	Specific heat capacity of air at film temperature
ρ	$0.5740\ kgm^{-3}$	Density of air at film temperature
k	$0.04629\ Wm^{-1}K^{-1}$	Thermal conductivity of air at film temperature
μ_f	$3.050 \times 10^{-5}\ kgm^{-1}s^{-1}$	Dynamic viscosity of air at film temperature

[Table 2: properties of air at the film temperature]

The properties of air in Tables 1 and 2 have been obtained using linear interpolation from [1, pp.11].

2.1.2 Preliminary Calculations

This section covers the empirical calculations for calculating the minimum required air velocity.

The surface area of the sphere (A), calculated using Equation (2), represents the total area over which the heat (Q) is being transferred.

$$A = \pi D^2 = 7.85 \times 10^{-3}\ m^2 \text{ (2)}$$

Newton's Law of Cooling, shown by Equation (3), can be used to determine the required convective heat transfer coefficient (h) that must be achieved by the air flow to dissipate the heat.

$$Q = hA(T_s - T_\infty) \text{ (3)}$$

$$h = \frac{Q}{A(T_s - T_\infty)} = 60.63\ Wm^{-2}K^{-1}$$

The Prandtl number can be calculated using Equation (4); it is a dimensionless ratio between the momentum diffusivity and thermal diffusivity; it compares how fast motion spreads within the fluid to how fast heat spreads. It also appears in both heat transfer correlations.

$$Pr = \frac{C_p \mu_f}{k} = 0.6937 \text{ (4)}$$

Additionally, the Nusselt number, obtained through Equation (5), is a dimensionless ratio between the convective and conductive heat transfer across the boundary layer, and is directly related to the convective heat transfer coefficient.

$$Nu = \frac{hD}{k} = 65.49 \text{ (5)}$$

As $Nu >> 1$, this signifies the heat transfer taking place is dominated by convection.

2.1.2.1 Ranz-Marshall Correlation

The Ranz-Marshall correlation [2, eq.(6)], represented by Equation (6), is one of the simplest forms. It is suitable for preliminary estimates, and can be used to predict the Nusselt number for convective heat transfer over a sphere, however it is cited for lower Reynolds numbers $(Re < 200)$[2, Ch1.2].

$$Nu = 2 + 0.6Re^{1/2}Pr^{1/3} \text{ (6)}$$

$$Re = 14290$$

$$U = \frac{\mu Re}{\rho D} = 15.18\ ms^{-1} \text{ (7)}$$

After calculating the minimum required velocity using Equation (7) to ensure the sphere surface does not exceed the threshold temperature, Equation (9) can be used to calculate the expected drag force (F_D). However, the drag force is calculated using the coefficient of drag (C_D), which depends on the Reynolds number. The coefficient of drag value was obtained using the C_D vs Re curve [3] for drag on a smooth sphere (0.427). The reference area shown by Equation (8) used to calculate the drag coefficient for a sphere is its projected frontal area (A).

$$A = \frac{\pi D^2}{4} = 1.96 \times 10^{-3}\ m^2 \text{ (8)}$$

$$F_D = \frac{1}{2}\rho U^2 A C_D = 0.0554\ N \text{ (9)}$$

2.1.2.2 Whitaker Correlation

The fundamental difference between the Whitaker [2, eq.(4)] and Ranz-Marshall correlation is the inclusion of the viscosity ratio in Whitaker's correlation, shown by Equation (10). This correlation is considered to be more accurate, as fluid viscosity varies with temperature. In addition, the Reynolds number expression is split up into two terms, each representing one of the regimes that develop in the laminar and wake regions during particle-fluid interactions. The Whitaker correlation can introduce issues occurring when $T_s - T_\infty > 800\ K$, for which the Wiskel and Henein correlation accounts for, however in this case the temperature difference is not great enough for it to be required [2]. It must be noted that while the Reynolds number validity ranges from $3.5 \times 10^4 \leq Re \leq 7.6 \times 10^4$, the correlation is only valid for viscosity ratios in the range $1.0 \leq (\frac{\mu_\infty}{\mu_s}) \leq 3.2$ - the ratio obtained in this experiment is 0.46. The range of validity for the Prandtl number is also cited at $0.71 \leq Pr \leq 380$, meaning the obtained empirical value of 0.6937 falls just outside.

$$Nu = 2 + (0.4Re^{1/2} + 0.06Re^{2/3})Pr^{0.4}(\frac{\mu_\infty}{\mu_{s,max}})^{1/4} \text{ (10)}$$

$$Re = 16180$$

$$U = \frac{\mu Re}{\rho D} = 17.19\ ms^{-1}$$

The expected drag force on the sphere can be determined again using the drag force curve [3] and Equation (9), however the coefficient of drag changes slightly due to the different Reynolds numbers. The coefficient of drag value used for this correlation is 0.433. The projected frontal area remains the same.

$$F_D = \frac{1}{2}\rho U^2 A C_D = 0.0720\ N$$

2.1.2.3 Raithby Correlation

This correlation [4, eq.(7)], represented by Equation (11), was developed based on experimental data where the Reynolds number was in the range $3.6 \times 10^3 < Re < 5.2 \times 10^4$ using sphere diameters of 1.27, 2.54 and 5.08 cm. The maximum reported deviation between measurements and results of this correlation is 2%. The conditions used to develop this correlation are very similar to those of this experiment, making it a very suitable choice, however it is important to note that this is not yet a widely accepted correlation.

$$Nu = 2 + 0.21Re^{0.61} \text{ (11)}$$

$$Re = 11650$$

$$U = \frac{\mu Re}{\rho D} = 12.34\ ms^{-1}$$

Again, the same curve [3] is used with Equation (9) to determine the drag force, however the coefficient of drag changes slightly; the value used for this correlation based on the Reynolds number is 0.416. The projected frontal area remains the same.

$$F_D = \frac{1}{2}\rho U^2 A C_D = 0.0356\ N$$

2.1.3 Critical Analysis

The results show a significant spread in the required velocity and corresponding drag, ranging from lower values of 12.34 ms^{-1} and 0.0356 N (Raithby) to 17.19 ms^{-1} and 0.0720 N (Whitaker). This constitutes an uncertainty range of 39.3% in required velocity and 102% in drag - there is large variation between correlations. The CFD simulation should fall within or near this range.

It is important to note that the empirical results are also subject to further uncertainty primarily due to property data and correlation assumptions. The properties of air cited above were obtained by linear interpolation between known, tabulated values. This introduces uncertainty because these properties vary non-linearly with temperature, particularly viscosity and thermal conductivity. For example, if the interpolated values underpredict viscosity, the calculated velocity would be lower. Additional uncertainties arise from assuming constant properties at the film temperature and neglecting radiation, which would reduce the required convective heat transfer. The overall impact of these uncertainties is not monumental but reinforces the idea that empirical results represent an approximation rather than an exact value, hence emphasising the importance of comparison with CFD simulations.

The Ranz-Marshall correlation may be suitable for quick, preliminary estimations - however it is only valid for lower Reynolds numbers, making it a poor choice in this experiment. Although the Whitaker equation is structurally superior due to the viscosity ratio, the Prandtl number and viscosity ratio lie outside the correlation's cited range of validity, suggesting the result of 17.19 ms^{-1} is a poor estimation caused by extrapolation.

The Raithby correlation has a validated Reynolds number range that encapsulates the resulting Reynolds number from all three calculations. However, its simplicity, similar to that of the Ranz-Marshall correlation, means it does not have a viscosity ratio, and does not cite the Prandtl number at all in the correlation. This suggests it does not account for the fluid's ratio of momentum diffusivity to thermal diffusivity. Its credibility can also be questioned, as it is not a widely accepted or known correlation, despite its maximum reported deviation between measurements and results being 2%.

Based on credibility and complexity, the Whitaker correlation appears to be the most suitable, suggesting that the empirical values for minimum required velocity and subsequent drag force to ensure no part of the sphere's surface exceeds the specified temperature, are 17.19 ms^{-1} and 0.0720 N respectively. These empirical results provide a baseline range that will be compared against CFD simulation data to assess model accuracy.

3.1 Simulation Procedure

3.1.1 Geometry

The computational domain was constructed to represent forced convection over a heated sphere. A sphere of diameter 50mm was placed within a larger fluid region, which represents the fluid domain. It is essential that the domain is large enough and the boundary regions are far enough away from the sphere so that the boundary conditions assigned to the outer domain do not alter the flow next to it and affect the quality of results [5]. To prevent this from occurring, the downstream distance was extended significantly (>5D), while the upstream and lateral boundaries were also sufficiently sized (>2D). This ensures the inlet velocity profile develops and resolves appropriately during the course of interaction with the sphere.

3.1.2 Mesh

A tetrahedral mesh was generated for the fluid domain, with refined inflation layers around the sphere to increase resolution at the boundary layer and break down complex geometry into more manageable elements. Accurate prediction of convective heat transfer relies heavily on near-wall behaviour, so the first layer thickness and growth rate were chosen to achieve $y^+ \approx 1$ for the selected turbulence models. This in combination with a sufficient number of layers ensures the steep velocity and temperature gradients can be resolved effectively. The mesh was also gradually coarsened away from the sphere to reduce computational cost while preserving accuracy in regions close to the sphere.

Mesh quality was assessed primarily using skewness, which is most important for a tetrahedral mesh [6]. Ideally, average skewness of a mesh falls below 0.33; from the skewness quality graph shown in Figure 1, the vast majority of elements have skewness < 0.2, indicating a very high-quality mesh.

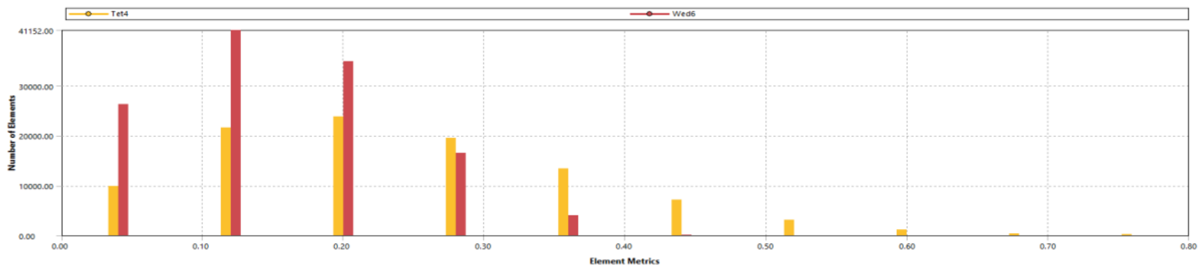

[Figure 1: Mesh Element Skewness]

Orthogonal quality shown in Figure 2 is not as crucial for a tetrahedral mesh. However, the mesh quality assessed using this metric still scores very high, with the majority of elements having quality > 0.8.

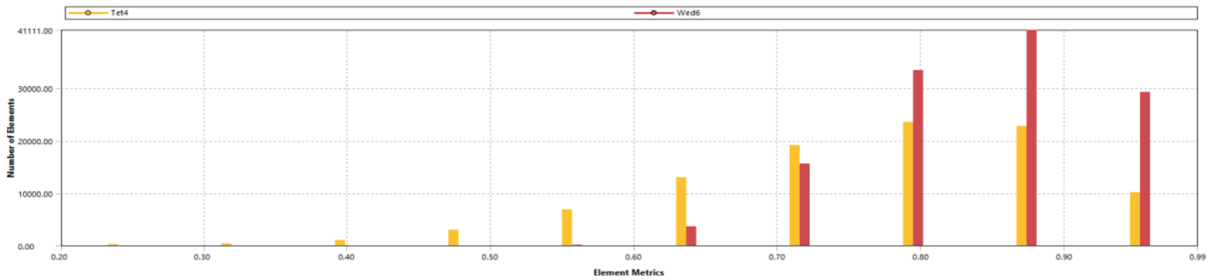

[Figure 2: Mesh Element Orthogonal Quality]

3.1.3 Mesh Sensitivity Analysis

A mesh sensitivity analysis was performed to quantify the influence of mesh density on the results. To ensure the quality of the boundary layer was affected more greatly than the remaining fluid region, the curvature angle was adjusted to increase the number of elements in the near-wall region, thus improving the sphericity of the body. The results of this procedure determine a mesh resolution that offers an acceptable balance between accuracy and computational cost. All simulations were carried out using the same turbulence model and inlet velocity so that the differences in output could be attributed solely to mesh resolution. Convergence was assessed by monitoring changes in maximum surface temperature.

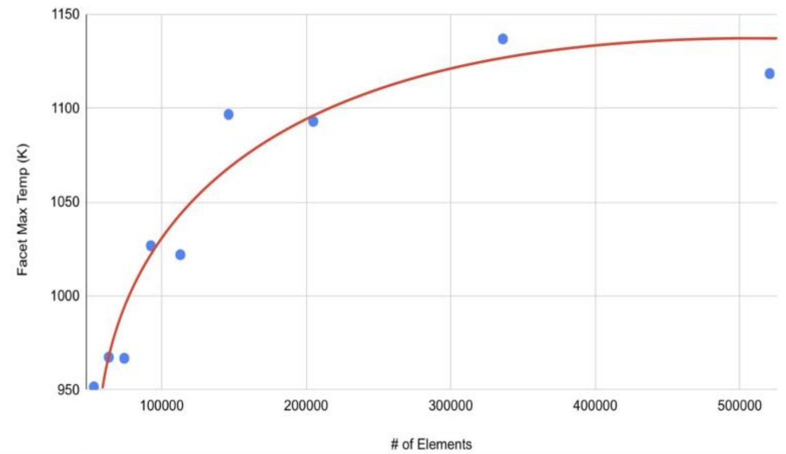

[Figure 3: Mesh Sensitivity Analysis]

The results in Figure 3 show that as the mesh is further refined, the results of the simulation begin to converge. To ensure a high level of accuracy while also maintaining a low computational expense, future simulations will be carried out at around 230,000 elements, stemming from a curvature angle of 3.8°.

3.1.4 Simulation

The simulations were configured to model external forced convection over the heated sphere using either constant-property air (evaluated at the film temperature) or ideal-gas density. A heat flux corresponding to the 300 W heat release ($q = \frac{Q}{A} = \frac{300}{\pi \times 0.05^2} = 38{,}200\ W/m^2$) was imposed on the sphere surface, which remained constant throughout. Turbulence models were selected based on expected flow behaviour:

- The $k - \omega\ SST$ model is a combination of $k - \omega$ and $k - \varepsilon$ models, and the widely accepted standard industry model used for accurate flow separation; it uses the strengths of $k - \omega$ for resolving near-wall and $k - \varepsilon$ in the free stream region. [10]
- The $k - \varepsilon$ model on its own is most common and effective for turbulent conditions

The energy equation was also turned on to ensure the heat loss of the sphere could be evaluated. Turbulence intensity was set at 5%, a typical value for this scenario; it represents the variations in velocity in relation to the mean flow. When tested at various other similar intensities, the effects on drag were negligible. Second-order upwind schemes were used for the momentum, turbulence and energy equations to improve accuracy. The simulations are ideally carried out until convergence, however due to computational limitations, each simulation underwent 200 iterations.

For each model comparison, the inlet velocity was adjusted incrementally until the maximum surface temperature fell at approximately 923 K. The corresponding drag force, drag coefficient, and Reynolds number were recorded for comparison with the empirical predictions.

4.1 Analysis of Results

4.1.1 Turbulence Model

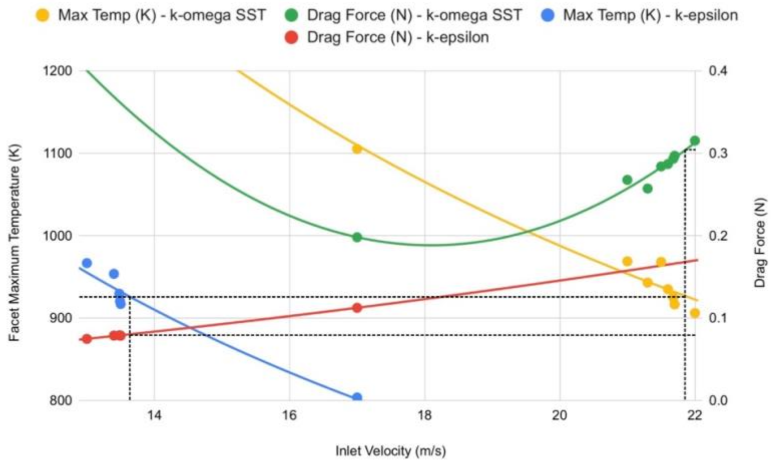

[Figure 4: Maximum Temperature & Drag Force vs Inlet Velocity using $k - \epsilon$ and $k - \omega$ SST models]

4.1.1.1 k-epsilon

Figure 4 shows that the simulations carried out using the $k - \varepsilon$ model experienced a steep decline in maximum surface temperature with increasing inlet velocity. The 923 K threshold is crossed at approximately 13.49 m/s, a relatively low value in comparison to empirical values. This may be due to the model's tendencies of over-predicting turbulent mixing, resulting in overly strong convection [7]. The required inlet velocity corresponds to a subsequent drag force of approximately 0.0787 N on the sphere. The drag force is modelled as a quadratic curve ($F_D \propto U^2$), and the maximum temperature as a power series curve ($T_s \propto \frac{1}{U^n}$).

4.1.1.2 k-omega SST

This model predicts a noticeably higher required velocity to sufficiently cool the sphere. Figure 4 shows that the required inlet velocity is approximately 21.76 m/s, subsequently causing a 0.302 N drag force on the sphere. The maximum temperature curve is more gradual over a larger range, which is consistent with the model's higher accuracy at boundary layers and use of model combinations depending on the region [8]. The sharper rise in drag occurs because the temperature threshold is reached at a higher inlet velocity. Compared to empirical expectations, this model provides the more physically credible results: higher required inlet velocity and drag values more consistent with flow over a sphere.

4.1.2 Density Model

Figure 5 shows a clear difference between the two density modelling approaches. The constant-density simulation used the film-temperature value of 0.574 kg/m³ - an artificially low value for representing the entire domain and weakens the convective cooling. As a result, the sphere is cooled to the threshold temperature by an inlet velocity of around 31.52 m/s, corresponding to a drag force of 0.263 N. On the other hand, the ideal-gas model allowed density to vary with temperature, producing average values around 1.174 kg/m³. The subsequent drag force was measured at a similar value (0.293 N), despite the required inlet velocity being only 21.7 m/s. This is because the density difference is so large that the proportionality of the force and square of the velocity is cancelled out.

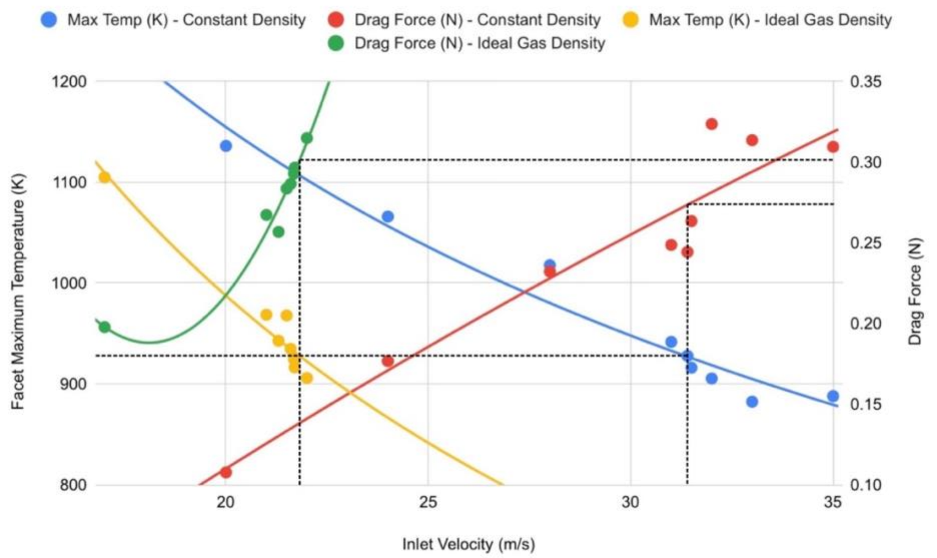

[Figure 5: Comparison of Maximum Temperature & Drag Force vs Inlet Velocity simulated at ρ_f and the ideal gas density using $k - \omega$ SST model]

4.1.3 CFD Limitations

Although these results provide valuable insight, there are several limiting factors that should be considered. Firstly, the mesh resolution, while tested for sensitivity, still compromises accuracy for computational cost. Additionally, the turbulence models themselves introduce large levels of uncertainty, as no model has the capability of perfectly replicating real conditions. For example, $k - \varepsilon$ is shown to be reliable for free-shear flows and preferred for high Reynolds number applications ($y^+ > 30$) [7], where separations and reattachments of flows are not present – making it a poor choice of model for this experiment. In contrast, $k - \omega$ SST still proves more applicable, however it is still known to overestimate turbulence in regions with normal strain. Furthermore, the simulations also neglect radiative heat transfer, which becomes significant at these temperatures, and would reduce the required convective cooling in a real system. In addition, the use of uniform inlet conditions and constant linearly interpolated material properties means the flow lacks real-world variability. Finally, the simulations were performed in steady-state mode, which cannot capture the vortex shedding known to occur at these Reynolds numbers; this may slightly underestimate drag fluctuations. These factors collectively limit the accuracy of the predictions and should be taken into account when analysing the results.

4.1.4 Validation & Verification

The empirical and CFD results show a substantial difference in the minimum required air velocity and subsequent drag force needed to maintain the sphere surface below 650°C. Being the most suitable model, the Whitaker correlation predicted a minimum required velocity of 17.19 m/s and a drag force of 0.0720 N. In contrast, the $k - \omega$ SST model predicted a higher required velocity of 21.76 m/s (27% increase) and a significantly higher drag force of 0.293 N (307% increase). This higher velocity is more reflective of its more realistic treatment of flow separation compared to $k - \varepsilon$, which underpredicted the required velocity (13.49 m/s), consistent with its tendency to overestimate turbulence. The large difference in drag force is likely primarily due to the computer's ability to vary air density as an ideal gas and calculate drag from resolved surface shear stresses and pressure. This results in a much higher and more accurate average density (1.174 kg/m³) as well as drag coefficient for the $k - \omega$ SST model (0.540) than the constant values used in the empirical calculations ($C_D = 0.433, \rho = 0.5740\ kgm^{-3}$), thus a greater subsequent drag force.

5.1 Conclusions & Recommendations

5.1.1 Conclusion

This study was carried out to determine the minimum air velocity required to prevent a sphere of diameter 50 mm and emitting 300 W heat, from exceeding a surface temperature of 650°C, while also quantifying the subsequent drag force. Empirical correlations predicted a required air velocity of 17.19 m/s and an associated drag force of 0.0720 N, providing a baseline comparison. The CFD simulations provided the necessary insight, revealing that the choice of turbulent model and density-variation approach significantly affects the cooling. Modelling density to vary with temperature, which was not considered in the empirical calculations, also proved to give a much lower required velocity but a greater, more accurate drag force. The $k - \varepsilon$ model underpredicted the required velocity due to turbulence overestimations, whereas the $k - \omega\ SST$ model provided a more realistic estimate of 21.76 m/s inlet velocity and 0.302 N drag force. Overall, CFD simulations offered a more realistic estimate than the solely empirical approach, but the combination of both provides an essential comparison.

5.1.2 Recommendations

It is imperative that these results are applied to the context of the situation; in a high-risk environment such as a nuclear power plant, mistakes and faults can be hugely expensive and dangerous. Therefore, further factors to improve the safety and efficacy of this application are recommended.

5.1.2.1 Streamlined Geometry

Although the sphere is a uniform, compact shape with low production costs, it is not aerodynamically efficient and produces a large separated wake in turbulent conditions. If the geometry is not required to remain spherical, a more aerodynamic shape, such as a teardrop is recommended. The aluminium support struts should also be manufactured to a streamlined shape, as streamlined geometry significantly reduces pressure drag and wake turbulence. The reduction in drag would reduce the mechanical load on the supports and reduce the required stiffness and manufacturing cost of the supports. The streamlined shape would also increase the effective convective surface area, potentially improving cooling performance and minimising the required inlet velocity. For example, a 5 m/s reduction would reduce blower power by 20-30%, thus lowering long-term operating costs.

5.1.2.2 Optimise Material Properties

Aluminium is far from an ideal choice of material for the supports due to its relatively low melting point (≈660°C). This leaves almost no leeway for safety margins given the maximum surface temperature of the sphere is 650°C. As the temperature of aluminium increases towards its melting point, it begins to experience strength loss, creep deformation and oxidation, all of which compromise its structural integrity. Over time, the weight of the sphere on the aluminium supports at high temperatures almost guarantees their failure. For this application, the supports should be constructed from a material with a higher melting point, yield strength, creep resistance and stiffness; stainless steel is a suitable option for the support material.

5.1.2.3 Inlet Flow Conditioning

It can be difficult to replicate a controlled simulation in real-life to achieve similar, accurate results, however one of the ways this can be helped is with flow conditioning. For example, the implementation of perforated plates would stabilise the incoming air flow and ensure a uniform inlet flow. This reduces the risk of local temperature excursions that could affect the structural integrity of the supports.

5.1.2.4 Surface Roughness

Surface roughness can be used strategically to improve the aerodynamic performance of the sphere. The addition of a rough surface rather than a smooth one promotes earlier transition from a laminar to turbulent boundary layer. This delays flow separation and reduces the size of the wake; this leads to the 'drag crisis'. The 'drag crisis' occurs at a lower Reynolds number for rougher surfaces than a smooth surface ($Re \approx 300{,}000$), causing the drag coefficient of a sphere to drop rapidly from roughly 0.5 to 0.2. The CFD simulations returned a Reynolds number of 41,800 at an inlet velocity of 21.76 m/s; Figure 6 [9] shows that the drag crisis occurs at around this point for a sphere with the roughness of a golf ball. Therefore, increasing the surface roughness of the sphere to be that of a golf ball would approximately half the drag coefficient, resulting in a drag force of approximately 0.151 N. This greatly reduces the load on the support structure, thus requiring weaker supports and saving costs.

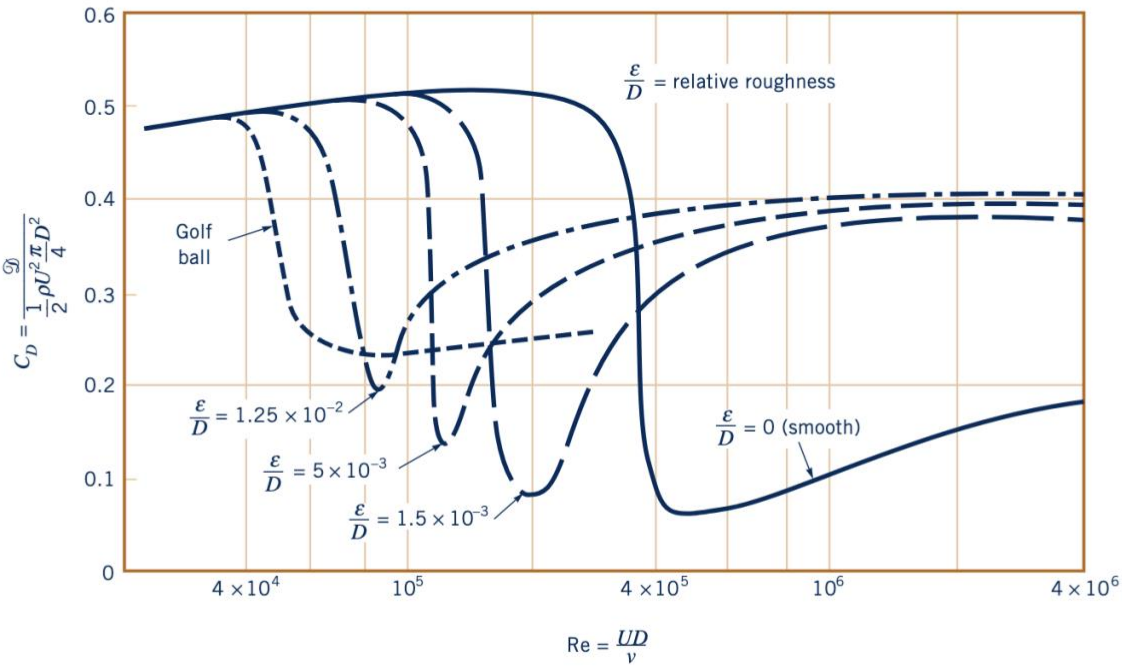

[Figure 6: Graphical comparison of 'Drag Crisis' at various levels of surface roughness]

5.1.2.5 Consideration of Radiation

As temperature increases, radiative effects become more and more significant, as per the Stefan-Boltzmann law ($E = \sigma T^4$). Therefore, improving the emissivity of the sphere - either by applying a high-emissivity coating or selecting a material with a naturally high emissivity - could greatly reduce the required cooling velocity. This is because a larger proportion of the heat transfer would occur via radiation rather than forced convection. As a result, the drag force acting on the sphere and supports would greatly reduce, and consequently the required stiffness and manufacturing cost.

References

[1] Faculty of Engineering, *The Little Book of Thermofluids*, 8th ed. University of Sheffield, Sep. 2024

[2] N. Ellendt, A.M. Lumanglas, S. Imani Moqadam and L. Mädler, "A model for the drag and heat transfer of spheres in the laminar regime at high temperature differences," *International Journal of Thermal Sciences*, vol. 133, pp. 98-105, Nov. 2018. [Online] doi: 10.1016/j.ijthermalsci.2018.07.009

[3] Drag Coefficient Calculator, "Interactive Summary Plot." Drag Coefficient Calculator https://kdusling.github.io/teaching/Applied-Fluids/DragCoefficientSummary.html (Accessed: Nov. 23, 2025)

[4] J.B. Will, N.P. Kruyt and C.H. Venner, "An experimental study of forced convective heat transfer from smooth, solid spheres," *International Journal of Heat and Mass Transfer*, vol. 109, pp 1059-1067, Feb. 2017. [Online] doi: 10.1016/j.ijheatmasstransfer.2017.02.018

[5] Ideal Simulations, "CFD Computational Domain." Ideal Simulations. https://www.idealsimulations.com/resources/cfd-computational-domain/#:~:text=CFD%20computational%20domain%20definition,discretised%20equations%20of%20fluid%20flows (Accessed: Nov. 23, 2025)

[6] Ansys, "6.2.2 Mesh Quality." Ansys Fluent Documentation. https://www.afs.enea.it/project/neptunius/docs/fluent/html/ug/node167.htm#:~:text=A%20good%20rule%20of%20thumb,could%20affect%20stability%20and%20accuracy (Accessed: Nov. 23, 2025)

[7] Simscale, "k-epsilon." Simscale. https://www.simscale.com/docs/simulation-setup/global-settings/k-epsilon/ (Accessed: Nov 23, 2025)

[8] Simscale, "k-omega-sst." Simscale. https://www.simscale.com/docs/simulation-setup/global-settings/k-omega-sst/ (Accessed: Nov. 23, 2025)

[9] B. Munson, T. Okiishi, W. Huebsch, A. Rothmayer, *Fundamentals of Fluid Mechanics, Seventh Edition,* fig.9.25 pp. 524, 2013.